

Simultaneous estimation of contact position and tool shape with high-dimensional parameters using force measurements and particle filtering

Journal Title
 XX(X):1–16
 ©The Author(s) 2016
 Reprints and permission:
sagepub.co.uk/journalsPermissions.nav
 DOI: 10.1177/ToBeAssigned
www.sagepub.com/

SAGE

Kyo Kutsuzawa¹ and Mitsuhiro Hayashibe¹

Abstract

Estimating the contact state between a grasped tool and the environment is essential for performing contact tasks such as assembly and object manipulation. Force signals are valuable for estimating the contact state, as they can be utilized even when the contact location is obscured by the tool. Previous studies proposed methods for estimating contact positions using force/torque signals; however, most methods require the geometry of the tool surface to be known. Although several studies have proposed methods that do not require the tool shape, these methods require considerable time for estimation or are limited to tools with low-dimensional shape parameters. Here, we propose a method for simultaneously estimating the contact position and tool shape, where the tool shape is represented by a grid, which is high-dimensional (more than 1000 dimensional). The proposed method uses a particle filter in which each particle has individual tool shape parameters, thereby to avoid directly handling a high-dimensional parameter space. The proposed method is evaluated through simulations and experiments using tools with curved shapes on a plane. Consequently, the proposed method can estimate the shape of the tool simultaneously with the contact positions, making the contact-position estimation more accurate.

Keywords

Intrinsic contact sensing, force-signal processing, robotic tool use

Introduction

When robots manipulate objects or use them as tools, they often need to recognize the contact states between the grasped objects/tools and the environment. For instance, when inserting a key into a keyhole, the robot must know the contact position and conditions of the key and lock. In addition, when cutting the bone-in meat with a knife, the robot must detect where the knife contacts with the bone. In such situations, robots need to detect contact states indirectly because tools usually have no sensors. Moreover, because tools hide the contact location, robots must estimate the contact information from force signals instead of vision.

Conventional methods for contact-position estimation from force signals require the shape and position of the tools. A technique for contact-position estimation (Salisbury 1984) often requires the shape of the tool surface to be known. However, shape measurements using cameras generally exhibit large errors in the depth direction and are sensitive to occlusion, reflection, and transparency. Although there are several methods for contact-position estimation without shape information (Tsuji et al. 2017; Koike et al. 2017), the estimation is slow, and these methods require that contact force constantly fluctuates during estimation. As those drawbacks are unavoidable unless using shape information, it is beneficial to estimate tool shape for estimating the contact position. Additionally, the shape of the

object/tool is necessary to assemble tasks and plan a control strategy (von Drigalski et al. 2020).

For tools made of transparent or reflective materials, it would be helpful to be able to estimate the tool shape from force signals instead of vision. Recently, a method that simultaneously estimates the contact position and tool shape from force signals was proposed (Kutsuzawa et al. 2020). This method gradually estimates the contact position and tool shape under uncertainty using an unscented particle filter (UPF) (van der Merwe et al. 2000a,b). However, it requires the tool shape to be expressed using a small number of parameters. It is practically impossible to apply that method to general shapes because the dimensionality of the tool-shape parameters becomes high, which requires an exponential number of particles for a reliable estimation. There is another method that can detect the contact position while estimating the tool shape of voxels from force measurements (Bimbo et al. 2022), but this method requires the geometry of the environment being static.

¹Department of Robotics, Graduate School of Engineering, Tohoku University, Japan

Corresponding author:

Kyo Kutsuzawa, Department of Robotics, Graduate School of Engineering, Tohoku University, 6-6-01 Aoba, Aramaki, Aoba-ku, Sendai, 980-8579, Japan.

Email: kutsuzawa@ieee.org

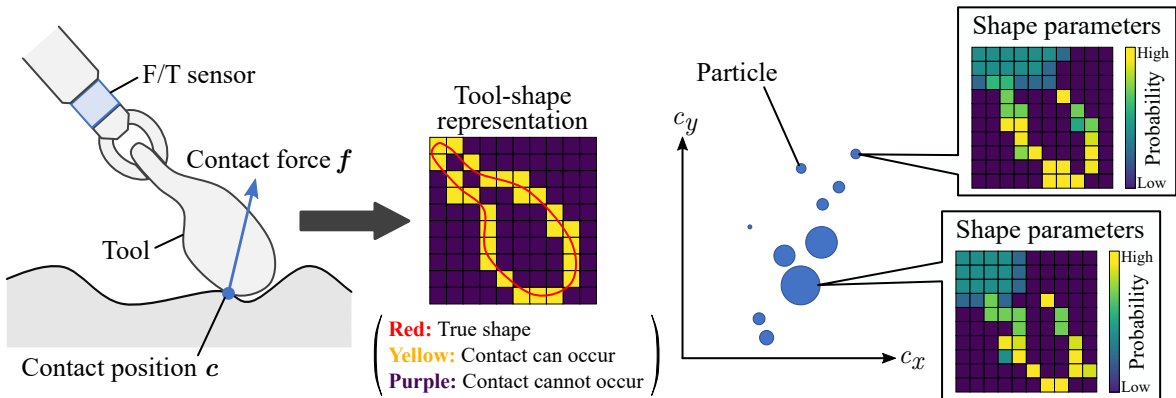


Figure 1. Method overview. **Left:** The proposed method assumes a single contact point on a rigid tool. **Middle:** The tool shape is represented as a grid map in which each cell encodes whether the tool surface exists in the cell. Here, yellow cells contain the tool surface, meaning a contact point can appear within the cell. **Right:** A particle filter estimates contact position using a set of weighted particles distributed in a space of contact position ($c \triangleq [c_x, c_y]^\top$ in the figure). Each particle has its own grid map that represents shape parameters. Each time a new observation is made, the particle filter updates coordinates of the particles, their weights, and shape parameters.

Here, we propose a method to estimate the tool shape with a large number of parameters from force signals while simultaneously estimating the contact position, based on the Rao–Blackwellized particle filter (RBPF) (Murphy 1999) used in SLAM (Murphy 1999; Grisetti et al. 2005, 2007). The conventional method (Kutsuzawa et al. 2020) is affected by *the curse of dimensionality* owing to the application of a particle filter to high-dimensional parameters. By contrast, the proposed method avoids this issue by associating shape information with individual particles rather than scattering particles into the shape-parameter space. Thus, the proposed method enables the tool shape to be expressed using a high-dimensional grid representation (voxels or pixels). In addition, in contrast with Bimbo et al. (2022), the proposed method does not need any assumption of environment geometry. Therefore, the proposed method is available even for the contact object in the environment being deformable and movable, e.g., a human touching the tool. In this study, we address the simple case of a curved object on a plane. Although simple, this setup can demonstrate the effectiveness of the proposed method because the challenge of this study is the high-dimensional shape parameter. The contributions of this study are listed as follows:

1. This study proposes a force-signal-based estimation method for tool shapes represented by high-dimensional variables (grid representation) without any assumptions of environment geometry.
2. We formulated a probabilistic model for contact position and tool-shape estimation from force signals.
3. This study also proposes a method for updating the tool-shape parameters represented by a grid using the estimated contact position and measurements.

Related Works

Salisbury first proposed a method for estimating the contact position using six-axis force/torque signals (Salisbury 1984). This method is based on the equilibrium of the force and

moment of force as follows:

$$\mathbf{F} = \mathbf{f}, \quad (1)$$

$$\mathbf{M} = \mathbf{c} \times \mathbf{f}, \quad (2)$$

where \mathbf{F} and \mathbf{M} indicate measured force and moment, and \mathbf{c} and \mathbf{f} indicate the contact position and force, respectively. From these equilibrium equations, \mathbf{c} can be determined as follows:

$$\mathbf{c} = \frac{\mathbf{F} \times \mathbf{M}}{\|\mathbf{F}\|^2} + \alpha \mathbf{F}, \quad (3)$$

where α is an unknown constant. This formulation implies that the contact position cannot be uniquely determined from the force signals. Instead, a line of contact-position candidates (*a line of action*) is determined. The method in Salisbury (1984) estimates the unique contact position to be the intersection of the line and tool surface as follows:

$$\mathbf{c} = \frac{\mathbf{F} \times \mathbf{M}}{\|\mathbf{F}\|^2} + \alpha \mathbf{F}, \quad \text{s.t. } g(\mathbf{c}) = 0. \quad (4)$$

A hypersurface with $g(\mathbf{p}) = 0$ represents the tool surface. Bicchi (1990) extended this method to soft-finger contacts. As these methods do not require arrayed tactile sensors and enable force/torque sensors to be placed far from the object surface where contact occurs, they can be applied to the contact estimation of external objects and tools. They can also be applied to the tactile sensing of robot bodies (Galvez et al. 2001; Iwata and Sugano 2002; Tsuji et al. 2009; Kim et al. 2021). The accuracy of contact-position estimation can be improved by combining other information, such as tool velocity (Muto and Shimokura 1993) and the derivative of force signals (Kitamura et al. 2017). Some studies have extended these methods to multiple-point contact (Featherstone et al. 1999; Kutsuzawa et al. 2015, 2016; Manuelli and Tedrake 2016), and these techniques have been applied to robot control (Featherstone et al. 1999; Park and Khatib 2008; Kutsuzawa et al. 2017; Benallegue et al. 2018).

Instantaneous measurements can only provide an estimate within the scope of (4), limiting the performance. Therefore,

as [Salisbury \(1984\)](#) suggested, past measurements can be used to improve contact-position estimation. [Kurita et al. \(2012\)](#) proposed a contact-position estimation method for non-convex shapes. Extending the method proposed in [Kurita et al. \(2012\)](#), [Tsuji et al. \(2017\)](#) proposed a contact-position estimation method without shape geometry. [Koike et al. \(2017\)](#) implemented this method using a particle filter.

These methods have also been extended to estimate geometric information. [Mimura and Funahashi \(1994\)](#) proposed a method for classifying contact states based on constrained degrees of freedom. [Karayannidis et al. \(2014\)](#) estimated the normal vector of a contact plane. [von Drigalski et al. \(2020\)](#) used a particle filter to identify the pose of a grasped tool with a known shape. [Liang et al. \(2022\)](#) used a particle filter to identify the pose and shape of a grasped tool based on the force signals. They also proposed a contact strategy to achieve fast estimation convergence. Although they achieved high-precision estimation, their method required the tool to be a rigid column of known length and the contact plane to be known. [Tsujimura and Yabuta \(1989\)](#) proposed a method for detecting the external object geometry from force signals by touching using a probe, while it requires a probe shape, and assumes that the contact position is uniquely determined. [Bimbo et al. \(2022\)](#) proposed a method that can reconstruct the geometry of tool and environment simultaneously with contact-position estimation. However, their method requires the geometry of the environment being static.

Although particle filters have often been used for the localization of external objects ([Chhatpar and Branicky 2005](#); [Petrovskaya et al. 2006](#); [Platt et al. 2011](#)), [Gadeyne et al.](#) proposed a particle filter for simultaneous contact state and geometrical parameter estimation from force signals and hand-tip positions ([Gadeyne et al. 2005](#)). They observed that the problem was similar to simultaneous localization and mapping (SLAM) ([Thrun et al. 1998](#)) and employed a particle filter to address the *chicken-and-egg* type estimation problem. Their concept is similar to that of this study, whereas the geometrical parameters were up to 12-dimensional (the positions/orientations of the manipulated and environment objects). The present study is based on [Kutsuzawa et al. \(2020\)](#) that proposed a method for the simultaneous estimation of contact position and tool shape. The method proposed in [Kutsuzawa et al. \(2020\)](#) can perform estimations only from force signals; however, the tool shape parameter is only approximately two-dimensional. Compared with these studies, the present study can handle high-dimensional (more than 1000 dimensions) shape parameters by employing techniques used in some SLAM methods ([Murphy 1999](#); [Grisetti et al. 2005, 2007](#)).

Method

Overview

The proposed method simultaneously estimates the contact position and tool shape using a particle filter. A particle filter is a Bayesian Monte Carlo technique that estimates variables based on the distribution of particles updated using Bayesian inference. However, the proposed method does not directly handle the space of the tool-shape parameters; instead, the tool-shape parameters are handled by associating them with

each particle. Therefore, the particles are distributed only in the contact-position space, making it easy to compute with a small number of particles, regardless of the dimensionality of the tool shape. An overview of this process is shown in Figure 1.

It should be noted that the proposed technique for handling high-dimensional shape parameters is based on the Rao–Blackwellized particle filter (RBPF) ([Murphy 1999](#)) used in SLAM ([Murphy 1999](#); [Grisetti et al. 2005, 2007](#)). In SLAM, the use of a grid map increases the number of dimensions of the variables to be estimated. An RBPF is designed such that each particle, with an individual grid map computed from its own estimate, is scattered only in the localization space. This significantly reduces the number of particles required. The proposed method applies this technique to intrinsic contact sensing by designing a probabilistic model and a novel shape-parameter update method, as described below.

Preliminary

Let the contact position at the time step k be $\mathbf{c}_k \in \mathbb{R}^3$. Additionally, let an observation variable $\mathbf{y}_k \in \mathbb{R}^6$ comprise force $\mathbf{F}_k \in \mathbb{R}^3$ and the moment of force $\mathbf{M}_k \in \mathbb{R}^3$ measured by a force/torque sensor. We assume that the following force equilibrium is maintained between the contact position and the measured values:

$$\mathbf{M}_k = \mathbf{c}_k \times \mathbf{F}_k. \quad (5)$$

This formulation assumed a single contact point with no torque at the contact point. Gravity and inertial forces were excluded from the measurements in advance. Note that this method can also be applied to two-dimensional cases by omitting the z -axis components of position and force as well as the x - and y -axes components of the moment of force.

We define the object-shape parameter as $\mathbf{s}_k \in \mathbb{R}^{N_s}$, where N_s indicates the number of object-shape parameters. We let \mathbf{s}_k be expressed by a grid map, where each cell takes 0 to 1; the value is 1 when the object surface is at the cell, and 0 for no object surface. This representation is high-dimensional; when a region of $30 \text{ cm} \times 30 \text{ cm} \times 30 \text{ cm}$ is filled with 1-cm cell size, the number of cells is $N_s = 30^3 = 27000$. This is an extreme high dimensionality compared with conventional studies ([Kutsuzawa et al. 2020](#); [Gadeyne et al. 2005](#)), in which the dimensions of the shape parameters were two or twelve.

For the sake of simplicity, we combined the variables to be estimated at time k , i.e. \mathbf{c}_k and \mathbf{s}_k , into a state variable \mathbf{x}_k as follows:

$$\mathbf{x}_k \triangleq (\mathbf{c}_k, \mathbf{s}_k). \quad (6)$$

Additionally, we denote $\mathbf{x}_{0:k}$ as a sequence of variables \mathbf{x} from the time step to 0 to k as follows:

$$\mathbf{x}_{0:k} \triangleq (\mathbf{x}_0, \mathbf{x}_1, \dots, \mathbf{x}_k). \quad (7)$$

This notation is also used for other time-series variables in the same way, e.g. $\mathbf{y}_{0:k} \triangleq (\mathbf{y}_0, \mathbf{y}_1, \dots, \mathbf{y}_k)$.

Probabilistic model

The generative model of the system is formulated in a recursive way as follows:

$$\begin{aligned} p(\mathbf{x}_{0:k}, \mathbf{y}_{0:k}) \\ = p(\mathbf{y}_k | \mathbf{x}_k) p(\mathbf{x}_k | \mathbf{x}_{k-1}) p(\mathbf{x}_{0:k-1}, \mathbf{y}_{0:k-1}), \end{aligned} \quad (8)$$

where

$$\begin{aligned} p(\mathbf{y}_k | \mathbf{x}_k) &= p(\mathbf{M}_k | \mathbf{c}_k, \mathbf{F}_k) p(\mathbf{F}_k), \\ p(\mathbf{x}_k | \mathbf{x}_{k-1}) &= p(\mathbf{c}_k | \mathbf{c}_{k-1}, \mathbf{s}_k) p(\mathbf{s}_k | \mathbf{s}_{k-1}). \end{aligned} \quad (9)$$

As we would like to know $\mathbf{x}_{0:k}$, the goal is to estimate the following expectation value:

$$\begin{aligned} \mathbb{E}_{\mathbf{x}_{0:k} \sim p(\mathbf{x}_{0:k} | \mathbf{y}_{0:k})} [\phi(\mathbf{x}_{0:k})] \\ = \int \phi(\mathbf{x}_{0:k}) p(\mathbf{x}_{0:k} | \mathbf{y}_{0:k}) d\mathbf{x}_{0:k}, \end{aligned} \quad (10)$$

where ϕ denotes an arbitrary function. For instance, by defining as $\phi(\mathbf{x}_{0:k}) = \mathbf{c}_k$ and $\phi(\mathbf{x}_{0:k}) = \mathbf{s}_k$, we can obtain the expected contact position and tool shape at time k , respectively.

Particle filtering algorithm

Naive particle filtering In the particle filters, the expectation of $p(\mathbf{x}_{0:k} | \mathbf{y}_{0:k})$ is replaced with the expectation of an arbitrary distribution $q(\mathbf{x}_{0:k} | \mathbf{y}_{0:k})$, which is referred to as *the proposal distribution*, as follows:

$$\begin{aligned} \mathbb{E}_{\mathbf{x}_{0:k} \sim p(\mathbf{x}_{0:k} | \mathbf{y}_{0:k})} [\phi(\mathbf{x}_{0:k})] \\ = \int \phi(\mathbf{x}_{0:k}) p(\mathbf{x}_{0:k} | \mathbf{y}_{0:k}) d\mathbf{x}_{0:k} \\ = \frac{\int \phi(\mathbf{x}_{0:k}) w_k q(\mathbf{x}_{0:k} | \mathbf{y}_{0:k}) d\mathbf{x}_{0:k}}{\int w_k q(\mathbf{x}_{0:k} | \mathbf{y}_{0:k}) d\mathbf{x}_{0:k}} \\ = \frac{\mathbb{E}_{\mathbf{x}_{0:k} \sim q(\mathbf{x}_{0:k} | \mathbf{y}_{0:k})} [\phi(\mathbf{x}_{0:k}) w_k]}{\mathbb{E}_{\mathbf{x}_{0:k} \sim q(\mathbf{x}_{0:k} | \mathbf{y}_{0:k})} [w_k]}, \end{aligned} \quad (11)$$

where w_k denotes a weight variable defined as follows:

$$w_k \triangleq \frac{p(\mathbf{y}_k | \mathbf{x}_{0:k}) p(\mathbf{x}_{0:k})}{q(\mathbf{x}_{0:k} | \mathbf{y}_{0:k})}. \quad (12)$$

Moreover, by assuming

$$\begin{aligned} q(\mathbf{x}_{0:k} | \mathbf{y}_{0:k}) &= q(\mathbf{x}_k | \mathbf{x}_{0:k-1}, \mathbf{y}_{0:k}) q(\mathbf{x}_{0:k-1} | \mathbf{y}_{0:k}) \\ &= q(\mathbf{x}_k | \mathbf{x}_{0:k-1}, \mathbf{y}_{0:k}) q(\mathbf{x}_{0:k-1} | \mathbf{y}_{0:k-1}), \end{aligned} \quad (13)$$

we can rewrite the weight variables as follows:

$$w_k = \frac{p(\mathbf{y}_k | \mathbf{x}_k) p(\mathbf{x}_k | \mathbf{x}_{k-1})}{q(\mathbf{x}_k | \mathbf{x}_{0:k-1}, \mathbf{y}_{0:k})} w_{k-1}. \quad (14)$$

Finally, the expectation of (11) is approximated by using the weighted mean of samples from the proposal distribution as follows:

$$\mathbb{E}_{\mathbf{x}_{0:k} \sim p(\mathbf{x}_{0:k} | \mathbf{y}_{0:k})} [\phi(\mathbf{x}_{0:k})] \approx \frac{\sum_{i=0}^{N-1} \phi(\mathbf{x}_{0:k}^{(i)}) w_k^{(i)}}{\sum_{i=0}^{N-1} w_k^{(i)}}, \quad (15)$$

where

$$w_k^{(i)} = \frac{p(\mathbf{y}_k | \mathbf{x}_k^{(i)}) p(\mathbf{x}_k^{(i)} | \mathbf{x}_{k-1}^{(i)})}{q(\mathbf{x}_k^{(i)} | \mathbf{x}_{0:k-1}^{(i)}, \mathbf{y}_{0:k})} w_{k-1}^{(i)}, \quad (16)$$

$$\mathbf{x}_k^{(i)} \sim q(\mathbf{x}_k^{(i)} | \mathbf{x}_{0:k-1}^{(i)}, \mathbf{y}_{0:k}). \quad (17)$$

Proposed particle filtering A naive particle filter is based on (15)–(17) to compute the expectation value using the average of the samples (particles). However, this is practically impossible owing to the high dimensionality of shape parameters. There are two main difficulties with this method: 1) Many particles are required for a valid approximation in (15), which is difficult to handle exponentially as the number of dimensions increases owing to the curse of dimensionality; 2) Updating the proposal distribution, which must handle $\dim \mathbf{x} \times \dim \mathbf{x}$ covariance matrices, is computationally heavy as $\dim \mathbf{x}$ increases. Therefore, the implementation of particle filtering must be modified to avoid sampling from shape-parameter space.

We first modify the proposal distribution as follows:

$$\begin{aligned} q(\mathbf{x}_k | \mathbf{x}_{0:k-1}, \mathbf{y}_{0:k}) \\ \triangleq q(\mathbf{c}_k, \mathbf{s}_k | \mathbf{c}_{0:k-1}, \mathbf{s}_{0:k-1}, \mathbf{M}_{0:k}, \mathbf{F}_{0:k}) \\ = q(\mathbf{c}_k | \mathbf{c}_{0:k-1}, \mathbf{M}_{0:k}, \mathbf{F}_{0:k}) q(\mathbf{s}_k | \mathbf{s}_{k-1}, \mathbf{c}_{k-1}, \mathbf{F}_{k-1}). \end{aligned} \quad (18)$$

Although this is an arbitrary decomposition, we can separate the probabilistic distribution of \mathbf{c}_k and that of \mathbf{s}_k .

We also define the following assumption: the shape parameter \mathbf{s}_k can be uniquely updated from the contact position \mathbf{c}_{k-1} and the measured force \mathbf{F}_{k-1} . This is reasonable because the contact position is always on the shape surface and the contact force vector is usually directed inward toward the object (i.e., only the pushing force can be applied). This assumption is formulated as follows:

$$\begin{aligned} q(\mathbf{s}_k | \mathbf{s}_{k-1}, \mathbf{c}_{k-1}, \mathbf{F}_{k-1}) \\ = \begin{cases} 1 & \text{if } \mathbf{s}_k = \psi(\mathbf{s}_{k-1}, \mathbf{c}_{k-1}, \mathbf{F}_{k-1}), \\ 0 & \text{otherwise,} \end{cases} \end{aligned} \quad (19)$$

where ψ denotes an update function of the shape parameter which is defined in detail later.

By employing this assumption, we can obtain particles $\{\mathbf{x}_k^{(i)}\}_{i=1,\dots,N}$ as follows:

$$\mathbf{c}_k^{(i)} \sim q(\mathbf{c}_k^{(i)} | \mathbf{c}_{0:k-1}^{(i)}, \mathbf{M}_{0:k}, \mathbf{F}_{0:k}), \quad (20)$$

$$\mathbf{s}_k^{(i)} = \psi(\mathbf{s}_{k-1}, \mathbf{c}_{k-1}, \mathbf{F}_{k-1}). \quad (21)$$

Here, superscript (i) indicates the index of the particles sampled from the proposal distribution. We use the UPF (van der Merwe et al. 2000a,b), which employs an unscented Kalman filter (UKF) (Julier and Uhlmann 1997; Wan and van der Merwe 2000), for implementing the proposal distribution, $q(\mathbf{x}_k^{(i)} | \mathbf{x}_{0:k-1}^{(i)}, \mathbf{y}_{0:k})$.

Then, we can compute (11) using (15), where

$$w_k^{(i)} = \frac{p(\mathbf{M}_k, \mathbf{F}_k | \mathbf{c}_k^{(i)}) p(\mathbf{c}_k^{(i)} | \mathbf{c}_{k-1}^{(i)}, \mathbf{s}_k^{(i)})}{q(\mathbf{c}_k^{(i)} | \mathbf{c}_{0:k-1}^{(i)}, \mathbf{M}_{0:k}, \mathbf{F}_{0:k})} w_{k-1}^{(i)}. \quad (22)$$

We modeled probabilistic distributions as follows:

$$p(\mathbf{M}_k, \mathbf{F}_k | \mathbf{c}_k^{(i)}) = p(\mathbf{M}_k | \mathbf{F}_k, \mathbf{c}_k^{(i)}) p(\mathbf{F}_k), \quad (23)$$

$$p(\mathbf{M}_k | \mathbf{F}_k, \mathbf{c}_k^{(i)}) = \mathcal{N}(\mathbf{M}_k; \mathbf{c}_k^{(i)} \times \mathbf{F}_k, \Sigma^M), \quad (24)$$

$$p(\mathbf{F}_k) = \text{const}, \quad (25)$$

$$p(\mathbf{c}_k^{(i)} | \mathbf{c}_{k-1}^{(i)}, \mathbf{s}_k^{(i)}) = p(\mathbf{c}_k^{(i)} | \mathbf{c}_{k-1}^{(i)}) p(\mathbf{c}_k^{(i)} | \mathbf{s}_k^{(i)}), \quad (26)$$

$$p(\mathbf{c}_k^{(i)} | \mathbf{c}_{k-1}^{(i)}) = \mathcal{N}(\mathbf{c}_k^{(i)}; \mathbf{c}_{k-1}^{(i)}, \Sigma^c), \quad (27)$$

$$p(\mathbf{c}_k^{(i)} | \mathbf{s}_k^{(i)}) = \frac{\exp \left[\text{Grid}_{\mathbf{s}_k^{(i)}}(\mathbf{c}_k^{(i)}) \right]}{\int \exp \left[\text{Grid}_{\mathbf{s}_k^{(i)}}(\mathbf{c}) \right] d\mathbf{c}}. \quad (28)$$

Here, $\mathcal{N}(\mathbf{x}; \boldsymbol{\mu}, \boldsymbol{\Sigma})$ indicates the probability distribution of \mathbf{x} following a Gaussian distribution with its mean $\boldsymbol{\mu}$ and its variance $\boldsymbol{\Sigma}$. $\Sigma^M = \sigma_M^2 \mathbf{I}$ and $\Sigma^c = \sigma_c^2 \mathbf{I}$ indicate the variance of the moment and contact position, respectively. Additionally, $\text{Grid}_{\mathbf{s}}(\mathbf{x})$ indicates the value of the cell of the grid \mathbf{s} that contains position \mathbf{x} .

Finally, we compute the particle filtering (right side of (15)) without sampling from the high-dimensional shape-parameter space. Instead, we sampled $\mathbf{c}_k^{(i)}$ from the proposal distribution and computed $\mathbf{s}_k^{(i)}$ for each particle.

In summary, the main difference between the naive and proposed filtering algorithms is the sampling strategy, as can be seen by comparing (17) and (20)–(21). In the naive particle filter, the proposal distribution q needs to handle a high-dimensional space, but in the proposed particle filter, by assuming a deterministic shape update rule, the proposal distribution only needs to handle a low-dimensional space instead.

Shape estimation

To estimate the shape information effectively, the design of the function ψ is important. We design ψ using the following two criteria.

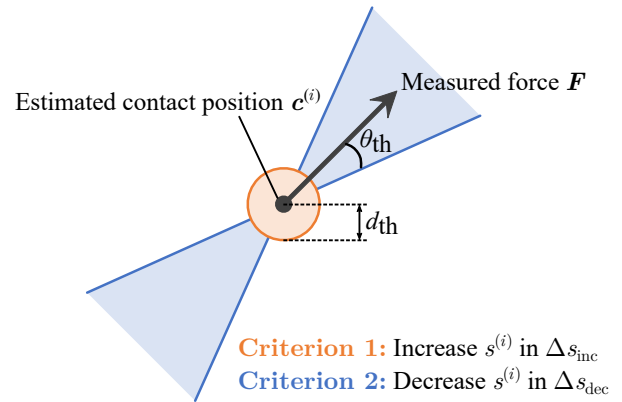
1. Tool surface exists around near the contact point \mathbf{c}_{k-1} .
2. Tool surface does not exist where it is far from \mathbf{c}_{k-1} along \mathbf{F}_{k-1} .

The first criterion was based on the fact that the contact position was always on a tool surface. The second criterion assists the estimation by reducing the existence of the tool shape at the point where no contact occurs. Because the contact provides only local information, the second criterion, which changes a wide range of shape information, can accelerate the estimation. An overview of these criteria is shown in Figure 2.

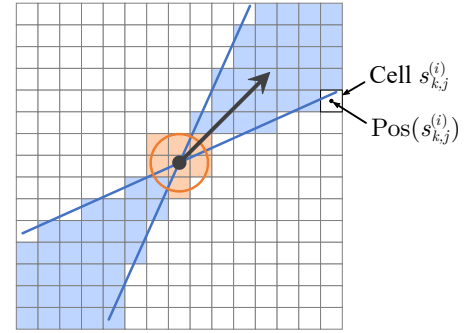
The first criterion is implemented as follows:

$$\begin{aligned} s_{k,j}^{(i)} &= s_{k-1,j}^{(i)} + \Delta s_{\text{inc}}, \\ \text{if } \|\text{Pos}(s_{k,j}^{(i)}) - \mathbf{c}_{k-1}^{(i)}\| &< d_{\text{th}}. \end{aligned} \quad (29)$$

Here, j indicates the cell index. Δs_{inc} and d_{th} indicate the increment of the shape parameter and the threshold of distance, respectively. $\text{Pos}(x)$ indicates the center position of cell x . This operation increases the values of the cell $s_{k,j}^{(i)}$ whose distance from the contact point $\mathbf{c}_{k-1}^{(i)}$ is less than d_{th} .



(a) Shape-estimation criteria.



(b) Grid-map increments.

Figure 2. Overview of tool-shape computation. (a) The criterion 1 (orange) increases shape parameters near the estimated contact position. The criterion 2 (blue) decreases shape parameters near the line of action expressed in (3) to accelerate shape estimation. (b) The value of each cell is updated when the center of the cell is within the area of the criteria 1 or 2. The grid map corresponds to those illustrated in Figure 1.

The second criterion is implemented as follows:

$$\begin{aligned} s_{k,j}^{(i)} &= s_{k-1,j}^{(i)} - \Delta s_{\text{dec}}, \\ \text{if } \text{Pos}(s_{k,j}^{(i)}) \in \text{cone}(\mathbf{c}_{k-1}^{(i)}, \mathbf{F}_{k-1}, \theta_{\text{th}}) \text{ and } \|\text{Pos}(s_{k,j}^{(i)}) - \mathbf{c}_{k-1}^{(i)}\| &\geq d_{\text{th}}. \end{aligned} \quad (30)$$

Here, $\text{cone}(\mathbf{a}, \mathbf{v}, \theta)$ indicates a double-cone with apex \mathbf{a} , axis along \mathbf{v} , and angle θ . Δs_{dec} and θ_{th} indicate the decrement of the shape parameter and the threshold of the angle, respectively. This operation decreases the values of cell $s_{k,j}^{(i)}$ that are near the line along \mathbf{F}_{k-1} through $\mathbf{c}_{k-1}^{(i)}$.

Simulation

Setup

We evaluated the proposed method through a simulation as illustrated in Figure 3. It simulated a robotic arm with an F/T sensor gripping a knife-shaped tool in a plane. The simulator was implemented by Python, and simulates the following contents. The contact surface has a shape defined as follows:

$$\{(x, y) | 0.1 \text{ m} \leq x \leq 0.3 \text{ m}, y = h(x)\}, \quad (31)$$

where $h : \mathbb{R} \rightarrow \mathbb{R}$ is a function that specifies the tool shape. The estimation was performed based on the coordinate

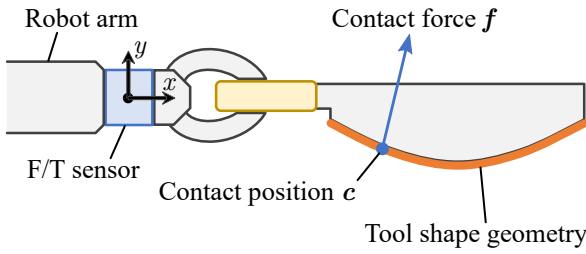


Figure 3. Setup for simulation. The simulation assumes that a robot arm with a force/torque sensor stably grasps a tool. The tool will contact with the environment at a single point within the orange area.

Table 1. Hyper-parameters of the proposed method in the simulation

Item	Symbol	Value
Number of particles	N	300
Size of grid cells	-	0.5 cm
Number of cells	N_s	80×80
Threshold of resampling	N_{th}	0.432
Std. of contact position	σ_c	5.25×10^{-4} cm
Std. of measured moment	σ_M	3.79×10^{-4} Nm
Threshold of distance	d_{th}	0.939 cm
Threshold of angle	θ_{th}	0.108 rad
Increment of shape params.	Δs_{inc}	0.0347
Decrement of shape params.	Δs_{dec}	0.0216

Table 2. Hyper-parameters of the baseline method in the simulation, where the symbols follow [Tsuji et al. \(2017\)](#)

Item	Symbol	Value
Forgetting factor	ρ	0.992
Regularization factor	α	860

Table 3. Hyper-parameters of the naive method

Item	Symbol	Value
Number of particles	N	300
Size of grid cells	-	8.0 cm
Number of cells	N_s	5×5
Threshold of resampling	N_{th}	0.432
Std. of contact position	σ_c	0.0114 cm
Std. of shape parameters	σ_s	4.37×10^{-3}
Std. of measured moment	σ_M	1.69×10^{-5} Nm

system of the F/T sensor. We assume that gravitational and inertial forces are eliminated. Thus, the estimation can be performed without considering robot motion.

Various external forces are applied at random positions on the tool surface. The contact force fluctuated in the first 10 s, but stopped fluctuating thereafter. During the task, the contact position $c = (c_x, c_y)$ changes every 1 s randomly. In the first 10 s, the contact force $f = (f_x, f_y)$ varies as follows:

$$f_x = A \sin \theta_f(t), \quad (32)$$

$$f_y = A \cos \theta_f(t), \quad (33)$$

$$\theta_f(t) = \theta_0 \sin(4\pi t) + \theta_{\perp}, \quad (34)$$

where the amplitude A changes every 1 s as follows:

$$A \sim U(1.0 \text{ N}, 3.0 \text{ N}). \quad (35)$$

θ_{\perp} indicates the angle normal to the tool surface at the contact position c_k , t indicates the time, and θ_0 indicates

the amplitude of contact force fluctuation. We set $\theta_0 = \frac{\pi}{6}$ unless otherwise specified. After 10 s, the contact force was maintained constant for 1 s and changed every 1 s as follows:

$$f_x = A \sin \theta_f, \quad (36)$$

$$f_y = A \cos \theta_f, \quad (37)$$

$$\theta_f \sim U\left(-\frac{\pi}{6}, \frac{\pi}{6}\right) + \theta_{\perp}. \quad (38)$$

We set the contact force vector within a certain angle of the tool surface normal, because stable contact requires the contact force vector to be within the friction cone.

The following three methods were used to compare the performance of contact-position and/or tool-shape estimation with the proposed method.

1. Baseline: contact-position estimation method that does not require shape information ([Tsuji et al. 2017](#)).
2. Naive: simultaneous contact-position and shape estimation with a naive particle filter ([Kutsuzawa et al. 2020](#)).
3. Oracle: contact-position estimation method where the actual tool shape is provided ([Salisbury 1984](#)).

The hyper-parameters are listed in Tables 1–3, that were selected by using Optuna ([Akiba et al. 2019](#)), a hyper-parameter optimization framework. Note that the Oracle method does not have hyper-parameters; it estimates contact positions based on (4).

The shape estimation errors were computed by selecting the highest-value cells along the y -axis and calculating the distance between the center of the cells and the y -axis position of the true shape surface.

$$e_{\text{shape}} \triangleq \frac{1}{M} \sum_{\mu=1}^M |h(x_{\mu}) - \text{Pos}(\arg \max_{\nu} s_{(\nu, \mu)})|. \quad (39)$$

Here, we did not use other common metrics for measuring differences between two shapes, such as Hausdorff distance. Hausdorff distance, for example, calculates the maximum distance from a point on one shape to the closest point on the other shape, that is sensitive to outliers. Also, common metrics generally require binarization in the continuous-valued shape parameters with an arbitrary threshold before they are applied. This metric, on the other hand, does not need any threshold.

Results

Performance of the proposed method

We first show the performance of the proposed method with tuned hyper-parameters. Also, we compared the proposed method with the other methods.

Figure 4 shows the progress of shape estimation in the proposed method in five types of shape. Also, Figure 5 shows the shape-estimation progress in the naive particle filter. In the proposed method, the tool-shape parameters gradually converged to near the true value. On the other hand, the naive particle filter failed to estimate the tool shape although the resolution was quite low. It should be noted that we could not run the naive particle filtering with $N = 300$ and $N_s = 6400$ in our computational environment since it required

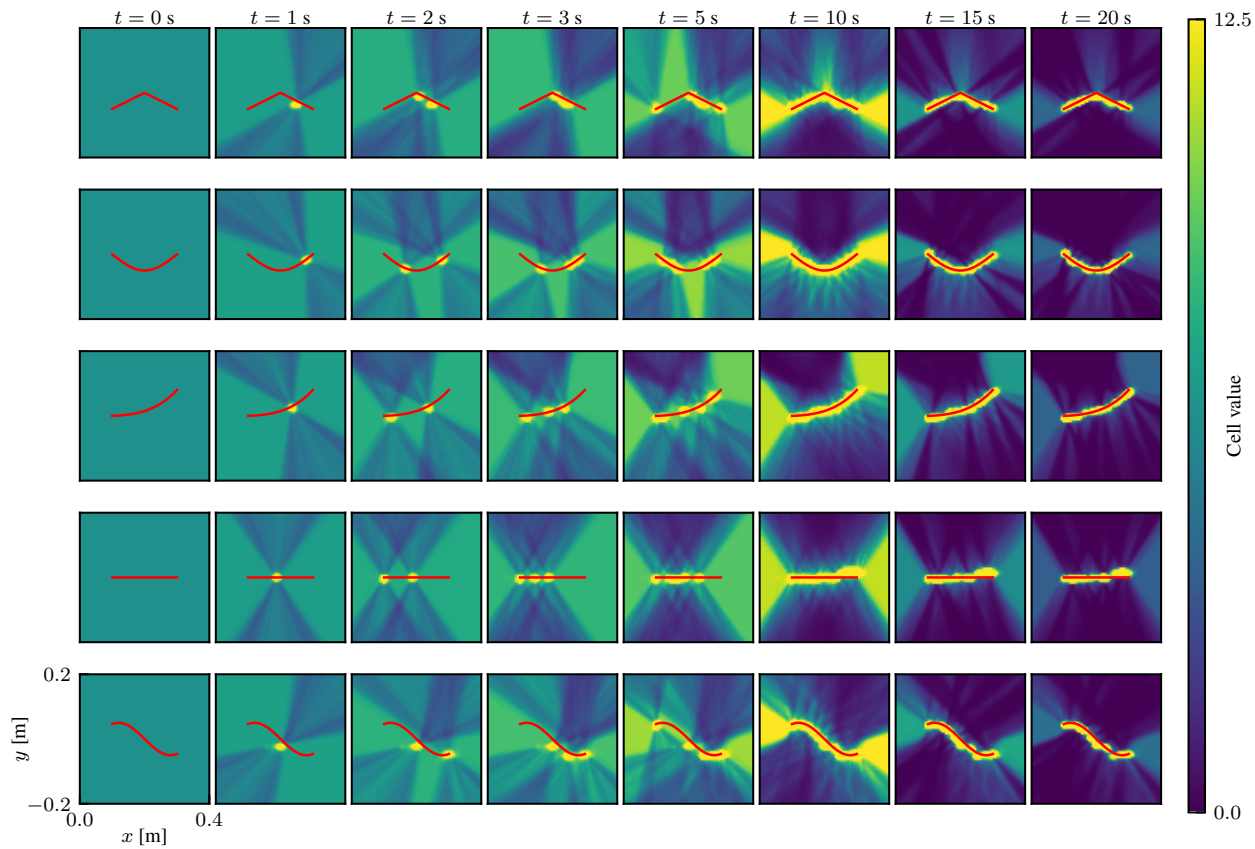


Figure 4. Progress of shape parameter estimation in the proposed method. The color maps represent the estimated tool shape, where yellow indicates a high degree of certainty that the tool surface is there (i.e., contact can occur). Red curves indicate the true object shape. Here, the cell value corresponds to s_k , and the value of 12.5 in the color bar was arbitrarily chosen for the sake of visibility in the color map.

approximately 366 GB of computer memory owing to the high-dimensionality of the state space. Table 4 compares shape-estimation errors in the proposed and naive methods in each shape. The proposed method resulted in approximately 0.5 cm of errors, whereas the naive method resulted in errors larger than 8 cm.

We then compared the estimation errors of contact positions between the proposed, naive, baseline, and oracle methods. Figure 6 shows the estimation errors for the 10 trials. The oracle method naturally achieved the highest performance, as it was provided with the true tool surface. We also observed that the proposed method outperformed the other methods.

Figure 7 presents the estimation results of contact positions in the proposed and baseline method. In the baseline method, the estimated contact position was unstable and did not converge to the true values after 10 s, when the contact force stopped oscillating. By contrast, the proposed method maintained approximately the same accuracy even after the contact force stopped oscillating.

Hyper-parameter evaluation

Up to this point, we have examined the performance of the proposed method in the optimized hyper-parameters listed in Table 1. Hereinafter, we investigate how the proposed method behaves as the hyper-parameters are varied.

We firstly evaluated varied resolution of shape parameters, N_s . Figure 8(a) shows the estimated shape parameters at

Table 4. Shape-estimation errors (means and standard deviations of 10 trials)

Shape	Errors [cm]	
	Proposed	Naive
Straight	0.540 ± 0.183	8.800 ± 2.680
Arch	0.608 ± 0.172	8.600 ± 3.191
Angular	0.568 ± 0.167	9.600 ± 3.809
Wavy	0.694 ± 0.177	9.867 ± 3.721
Knife	0.585 ± 0.132	10.035 ± 3.611

20 s. The proposed method could estimate even $N_s = 400 \times 400 = 160000$ dimensions of the shape parameter using 300 particles. In most cases, the shape surfaces were properly estimated regardless of the resolution. This demonstrates the ability of the proposed method to handle shape parameters with significantly higher dimensions than the number of particles. Figure 8(b) also shows the shape estimation errors with varying resolutions (cell sizes). The estimation errors increased as the cell size increased (i.e., the resolution becomes coarse) and finally converged to about a half of the cell size.

We then evaluated with different numbers of particles, N . Figure 9 shows the position-estimation errors for varying numbers of particles. Estimation errors decreased as the numbers of particles increase and almost converged in 300 particles.

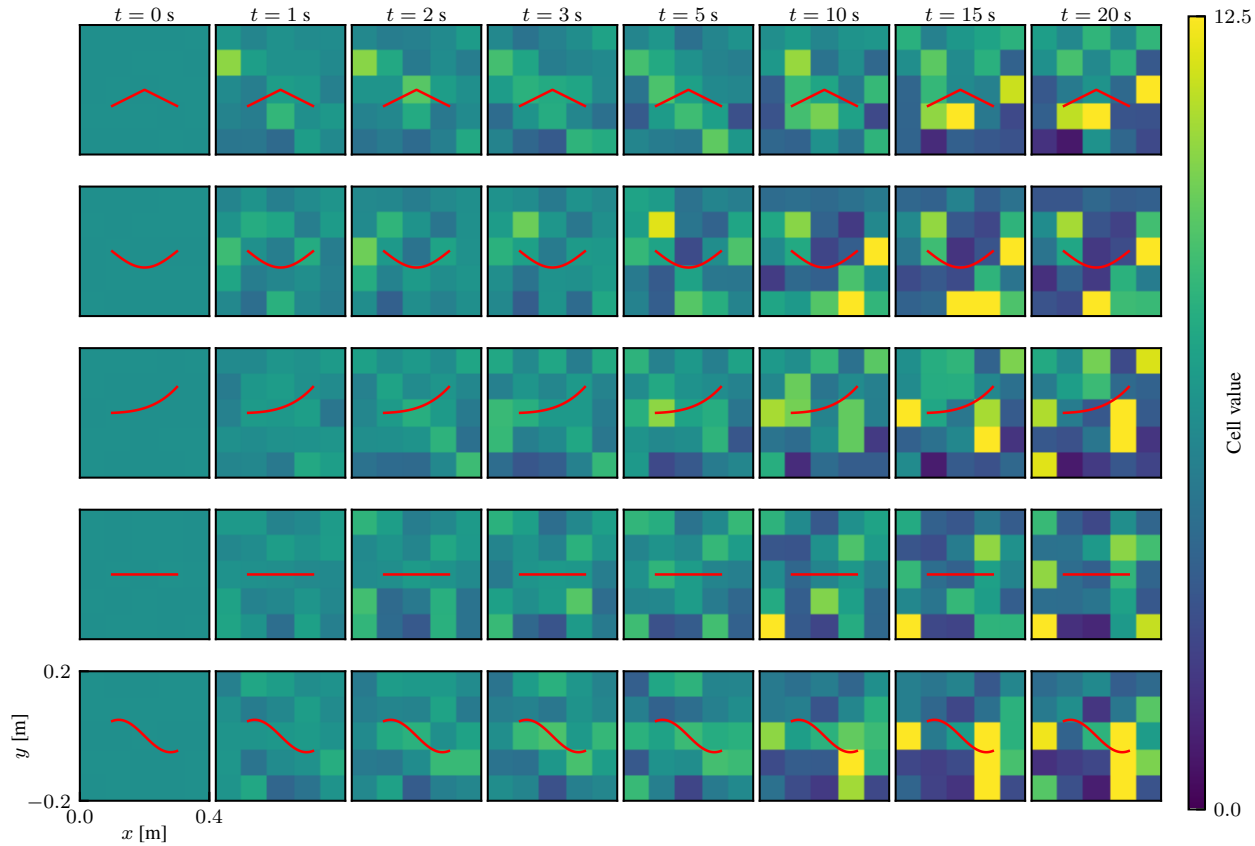


Figure 5. Progress of shape parameter estimation in the naive method. The color maps represent the estimated tool shape, where yellow indicates a high degree of certainty that the tool surface is there (i.e., contact can occur). Red curves indicate the true object shape.

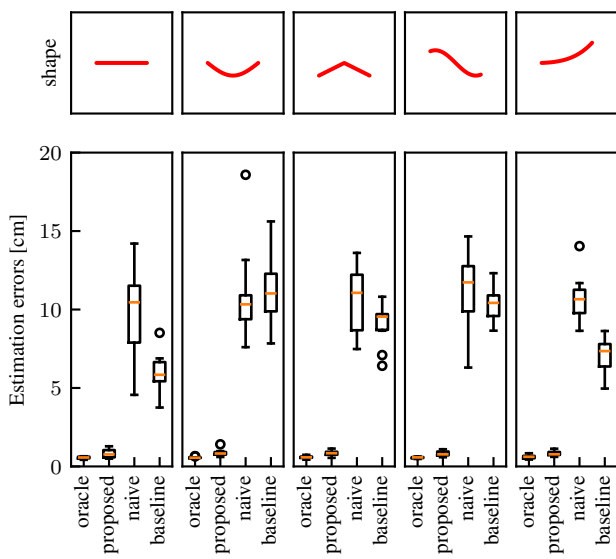


Figure 6. Estimation errors of the contact position after 10 s, where no fluctuation in contact force. Quartiles of 10 trials for each method and shape are shown.

We also evaluated hyper-parameters specific to the shape estimation. Figure 10 shows estimated shape parameters in the wavy-shaped tool with varying d_{th} and θ_{th} . Figure 11 shows estimated shape parameters in the wavy-shaped tool with varying Δs_1 and Δs_2 . For those parameters, the

Table 5. Specification of the F/T sensor (Source: <https://www.leptrino.co.jp/product/6axis-force-sensor>)

Item	Value
Rated capacity (force)	± 50 N
Rated capacity (torque)	± 0.5 Nm
Nonlinearity	$\pm 1.0\%$ R.O.
Cross-axis sensitivity	$\pm 2.0\%$ R.O.
Resolution	1/4000

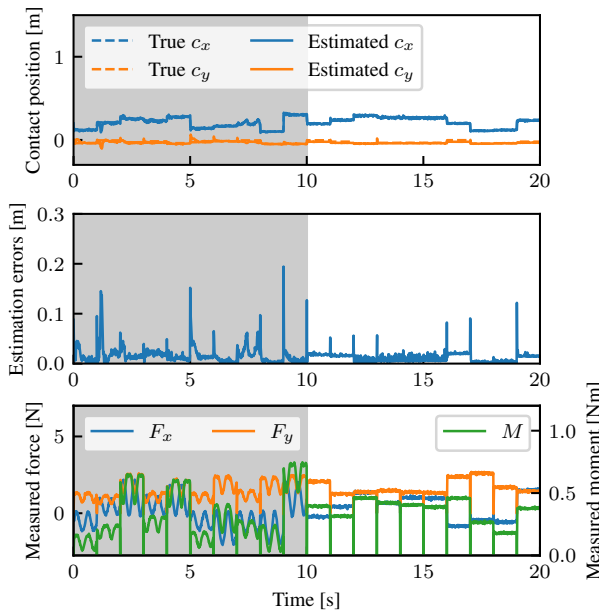
performance was degraded when the values were too large or too small.

The proposed method uses fluctuation of the contact force as a clue when the shape is totally unknown. Therefore, although not a parameter of the proposed method itself, we also evaluated with varying amplitude of force fluctuations, θ_0 . Figure 12 shows the estimation errors of contact position for varying amplitude of contact force fluctuation, θ_0 . We can observe that the estimation error increases as the fluctuation decreases.

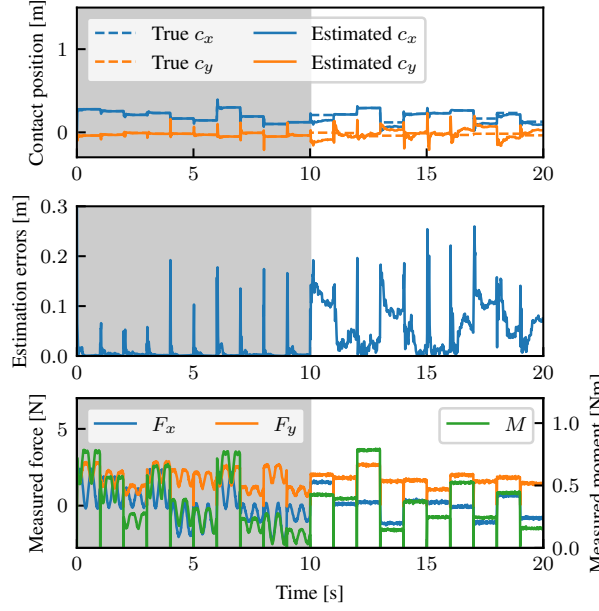
Experiment

Setup

Experiments were conducted using tools attached to a force/torque sensor, as shown in Figure 13. Although the sensor is on a fixture instead of a robot, this setup is equivalent to a situation in which a robot with an F/T sensor



(a) Proposed method

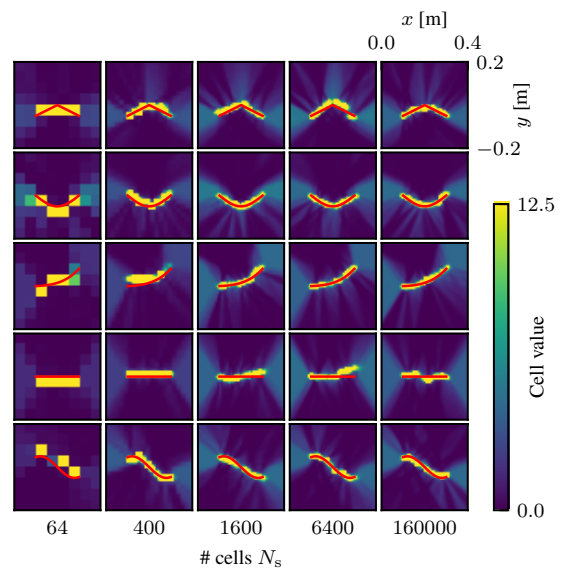


(b) Baseline method

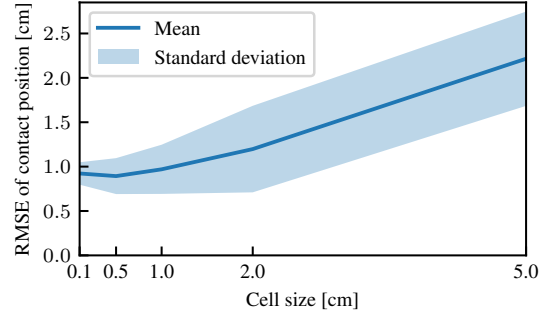
Figure 7. Estimated contact positions during simulation. The contact force intentionally fluctuated before 10 s (gray area), and then was maintained constant.

Table 6. Hyper-parameters of the proposed method in the experiments

Item	Symbol	Value
Number of particles	N	300
Size of grid cells	-	0.5 cm
Number of cells	N_s	80×80
Threshold of resampling	N_{th}	0.207
Std. of contact position	σ_c	5.64×10^{-4} cm
Std. of measured moment	σ_M	6.90×10^{-5} Nm
Threshold of distance	d_{th}	0.653 cm
Threshold of angle	θ_{th}	0.389 rad
Increment of shape params.	Δs_{inc}	0.0609
Decrement of shape params.	Δs_{dec}	0.0285



(a) Estimated shape parameters. The red curves indicate the true shapes of the tools.



(b) Position-estimation errors. The mean (solid curve) and standard deviation (filled area) of 10 trials are shown.

Figure 8. Estimation results with varying resolutions, N_s .

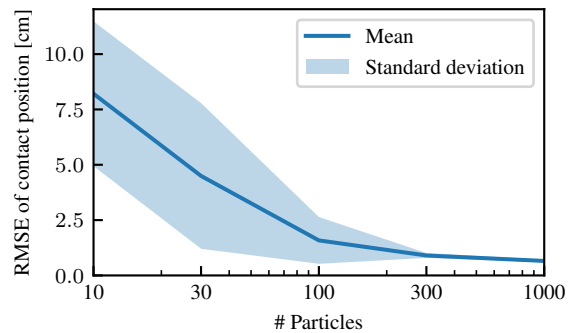


Figure 9. Estimation errors of the contact position with different numbers of particles, N . The mean (solid curve) and standard deviation (filled area) of 10 trials are shown.

Table 7. Hyper-parameters of the baseline method in the experiments, where the symbols follow [Tsuji et al. \(2017\)](#)

Item	Symbol	Value
Forgetting factor	ρ	0.979
Regularization factor	α	1.17×10^4

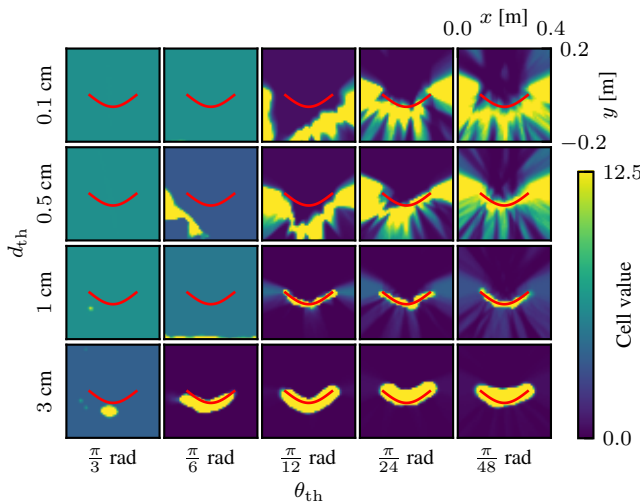


Figure 10. Estimated shape parameters with varying d_{th} and θ_{th} . The red curves indicate the true shapes of the tools.

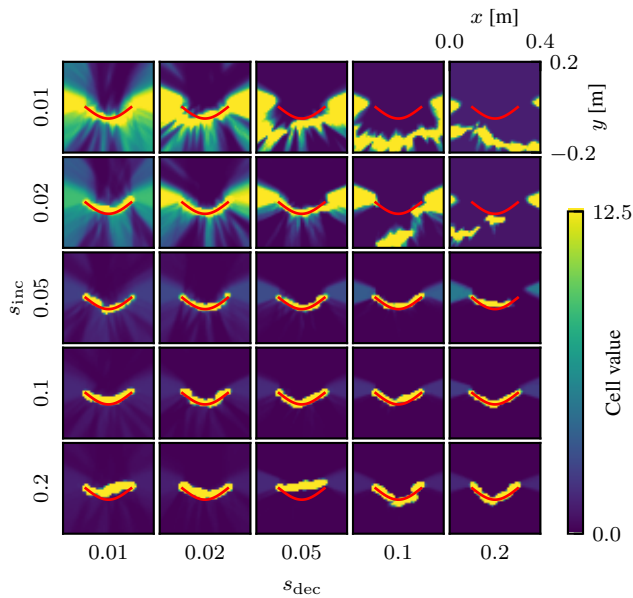


Figure 11. Estimated shape parameters with varying Δs_1 and Δs_2 . The mean values of all particles are shown. The red curves indicate the true shapes of the tools.

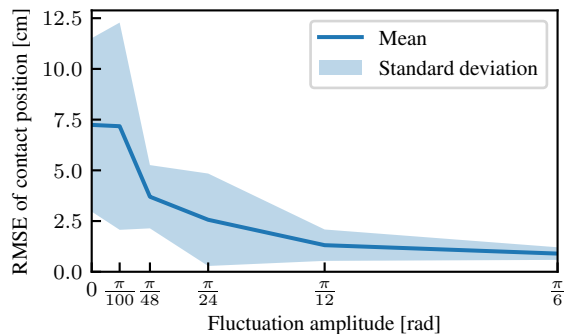


Figure 12. Estimation errors of the contact position with varying force-fluctuation amplitudes. The mean (solid curve) and standard deviation (filled area) of 10 trials are shown.

grips a tool (as illustrated in Figure 1) while gravity and inertial forces are eliminated. It should be possible to extend



Figure 13. Tools for the experiment. **Upper left:** Straight shape; **Upper right:** Angular shape; **Lower left:** Zigzag shape; **Lower right:** Discontinuous shape. Contact occurs only at the red-painted edges.

Table 8. Shape-estimation errors in the experiments (means and standard deviations of 5 trials of estimation with the same data)

Shape	Errors [cm]
Straight	0.395 ± 0.092
Angular	0.422 ± 0.116
Zigzag	0.701 ± 0.080
Discontinuous	0.476 ± 0.135

this setup to dynamic situations by identifying the inertia of the tool in advance using some method, such as Atkeson et al. (1986), and compensating for the gravity and inertial force. However, even with this setup, we can evaluate the essential topic of the present issue about how much the proposed method can estimate the tool shape and contact position from force signals.

We used a six-axis F/T sensor (PFS020YA500U6) supplied by Leptino, Inc. The basic specifications of the sensor are listed in Table 5. In the experiments, we only considered the y - z plane. The tools were straight- and angular-shaped with 15 cm long.

During measurement, the experimenter touched arbitrary positions on the edge of the tool and applied a contact force in various directions. Contact occurs at a single contact point at a time without large spin torque to maintain (5). Similar to the simulation, the contact force fluctuated for approximately 20 s and after that stopped fluctuating as much as possible.

In estimation, we regarded contact occurs when $\|\mathbf{F}\| \geq 0.5$ N. Once contact is lost, the estimation pauses, and the estimator is initialized except for the shape parameters. Hyper-parameters are listed in Tables 6 and 7, that were selected by using Optuna (Akiba et al. 2019).

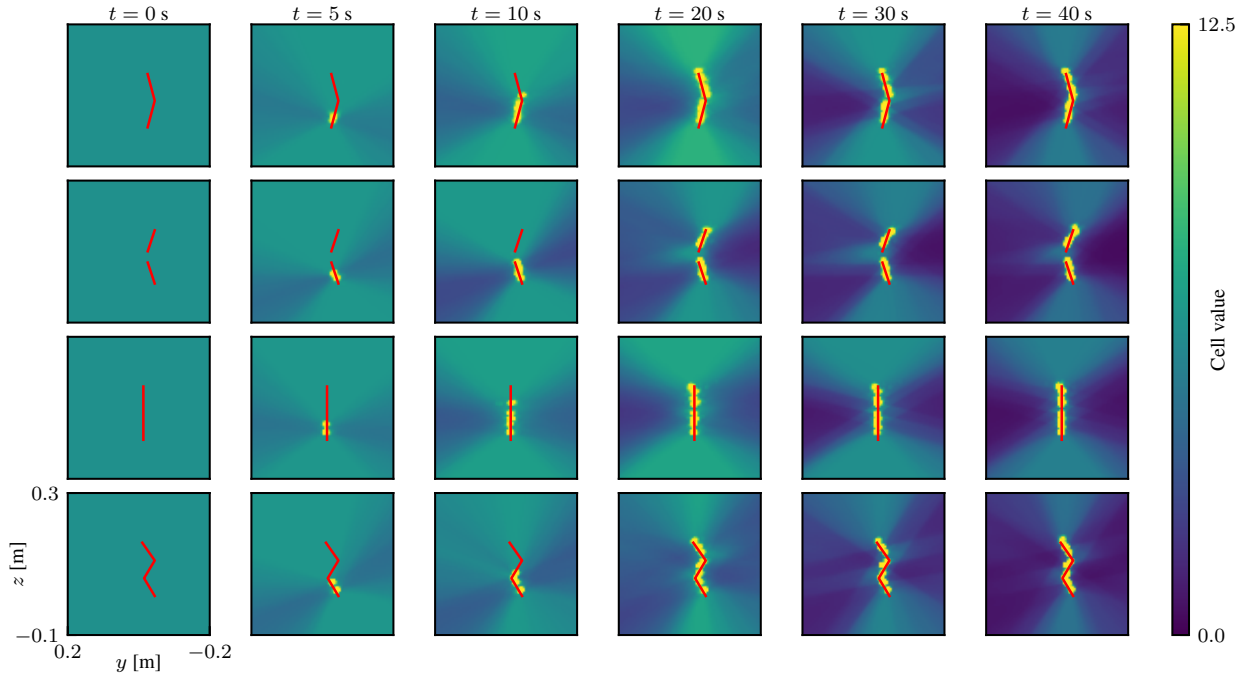
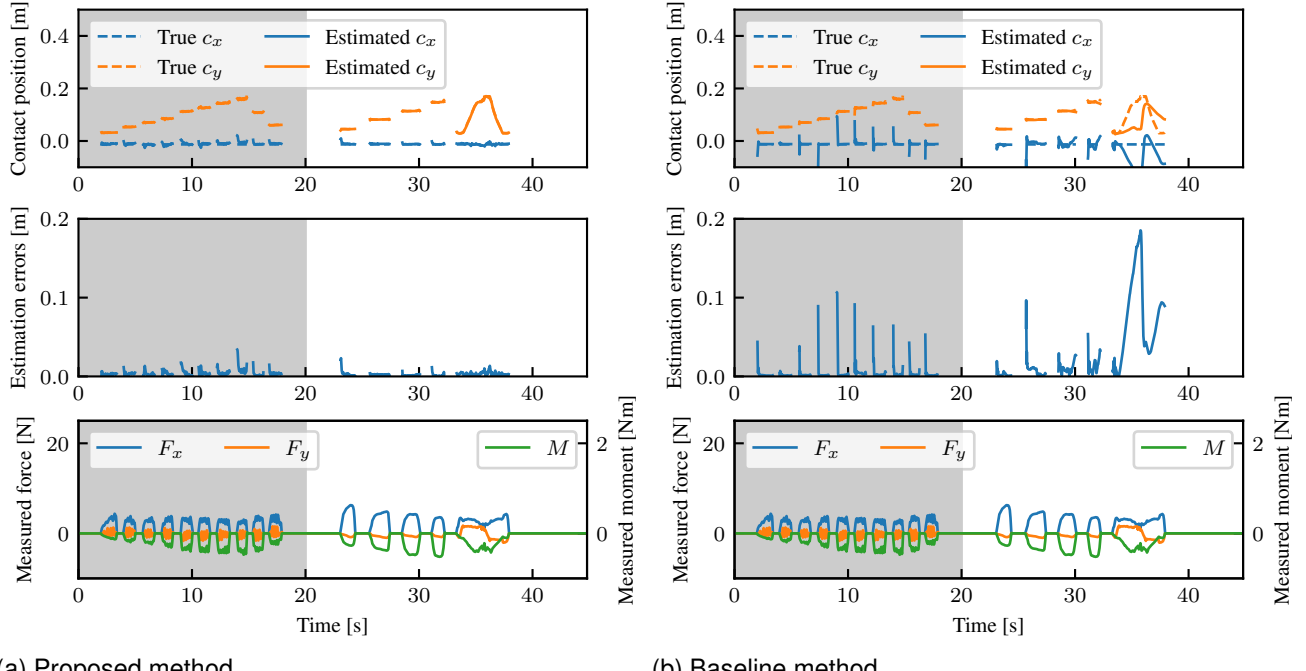


Figure 14. Progress of shape parameter estimation in the experiment. Red curves indicate the true object shape. The color maps represent the estimated tool shape, where yellow indicates a high degree of certainty that the tool surface is there (i.e., contact can occur).



(a) Proposed method

(b) Baseline method

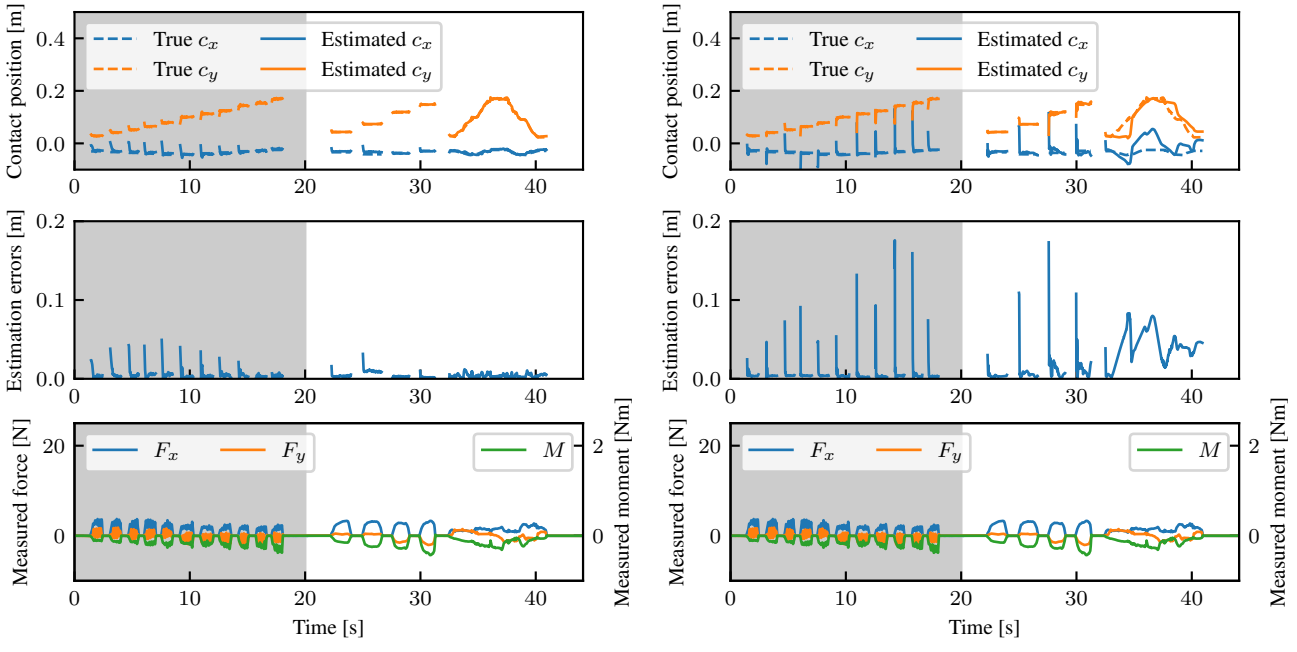
Figure 15. Estimated contact positions in the experiments with a straight-shaped tool. Dashed curves are estimated by the method with the tool shape being known (Salisbury 1984). The contact force intentionally fluctuated before 20 s (gray area), and then was maintained constant.

Results

Figure 14 shows the progress of the shape parameter estimation. The snapshots demonstrate that the tool-shape parameters gradually converged to near the true value. Table 8 shows shape-estimation errors in the proposed

method in each shape. The estimated shapes were generally within 1 cm of the actual shapes.

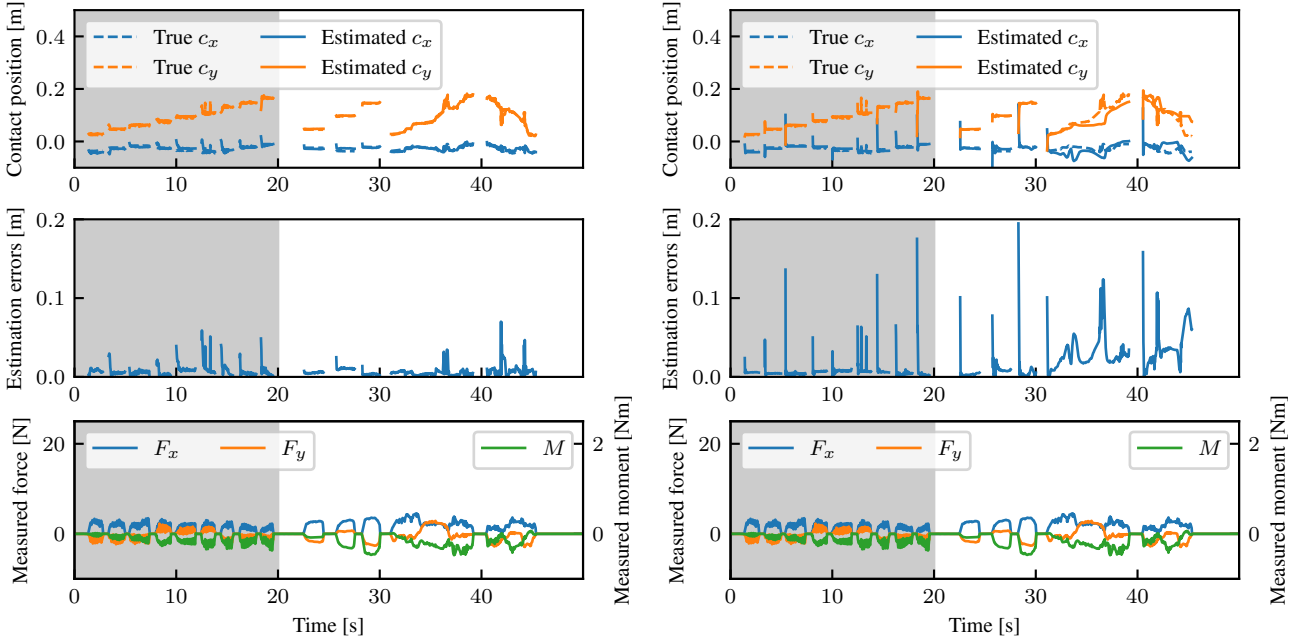
Figures 15–18 show the results of the contact-position estimation. Here, we used the oracle method for computing the actual contact positions. As a result, the proposed method could estimate contact positions with smaller errors than the



(a) Proposed method

(b) Baseline method

Figure 16. Estimated contact positions in the experiments with an angular-shaped tool. Dashed curves are estimated by the method with the tool shape being known (Salisbury 1984). The contact force intentionally fluctuated before 20 s (gray area), and then was maintained constant.



(a) Proposed method

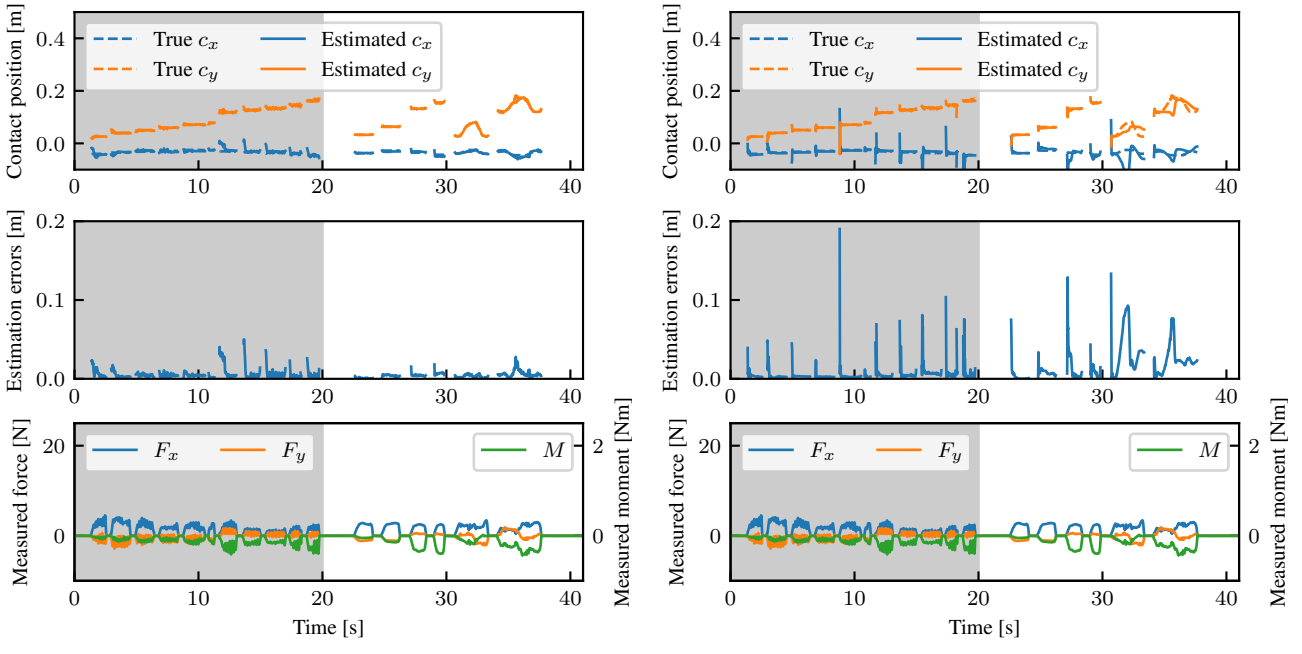
(b) Baseline method

Figure 17. Estimated contact positions in the experiments with a zigzag-shaped tool. Dashed curves are estimated by the method with the tool shape being known (Salisbury 1984). The contact force intentionally fluctuated before 20 s (gray area), and then was maintained constant.

baseline method. The contact position can be estimated even when the contact position moves rapidly without contact force fluctuations (after approximately 30 s). This is difficult for the baseline method because it requires contact force fluctuation and slow contact-position movement.

Discussion

The proposed method can estimate the contact position and tool shape starting from unknown values. The estimation process is as follows: The proposed method first estimates the contact position using the principle in Tsuji et al. (2017). This strategy is based on the assumption that the



(a) Proposed method

(b) Baseline method

Figure 18. Estimated contact positions in the experiments with a discontinuous-shaped tool. Dashed curves are estimated by the method with the tool shape being known (Salisbury 1984). The contact force intentionally fluctuated before 20 s (gray area), and then was maintained constant.

contact position moves slowly as contact force fluctuates. Using the estimated contact positions, the proposed method gradually estimated the tool shape ($t < 10$ s in Figure 4). Once tool shape estimation converged ($t \geq 10$ s in Figure 4), the proposed method can estimate contact position without contact force fluctuation. In addition, the proposed method does not need to switch between tool-shape estimation and contact-position estimation explicitly because both are performed simultaneously based on a framework of probabilistic inference. Although the estimation tends to proceed sequentially as mentioned above, both estimation processes always run simultaneously, and there is no need for those two steps to be clearly separated. Thus the proposed method is applicable to the situations where the contact force does not always fluctuate during tasks. This contrasts with the baseline method (Figure 7(b)), in which the contact-position estimation largely oscillated after the contact force fluctuation stopped. The same tendency was observed in the experimental results with an actual F/T sensor (Figures 14–18).

The proposed method can estimate the tool shape regardless of the parameter dimensions (i.e., grid resolutions), as shown in Figure 8. It is worth noting that the number of particles can be far smaller than the parameter dimensions. It was possible to handle shape parameters of the order of 10^5 by using the particle number of the order of only 10^2 . Although increased shape parameters needs a large computational cost, it will be still far efficient than the naive particle filtering and could be made more efficient by GPU parallelization. By contrast, some other hyper-parameters affect the estimation performance. First, the number of particles, N , strongly affects the performance, according to Figure 9. With a smaller number of particles it is easier

to fall into a sub-optimal local minimum, as there may be insufficient particle around appropriate estimates during the initial stages of estimation. Second, too small d_{th} and Δs_{inc} and too large θ_{th} may often result in collapsed shape estimation, according to Figures 10 and 11. Also, a large θ_{th} is considered to adversely affect the estimation for tool shapes with high curvature by decreasing cell values over a wide range. A small θ_{th} , on the other hand, slightly delayed the convergence of estimation. Third, preferred Δs_{dec} seem to depend on the magnitude of Δs_{inc} , according to Figure 11.

Comparison of the proposed method with the naive method suggests the effectiveness of the proposed shape-parameter update method, even apart from the dimensionality issue described above. The naive method resulted in poor performance in shape estimation even in a low-dimensional case, as shown in Figure 5. This would be because the naive particle filter treats variables (i.e. cells of the shape parameter and the contact position coordinates) as independent each other, ignoring their geometric relationship. Thus, the naive particle filter need to explore the entire space of the shape parameters including cells in a position that has nothing to do with the current contact positions. This is inefficient and would be easy to converge to a bad local minima. This may highlight the effectiveness of the proposed shape update method ((29), (30), and Figure 2) that utilize the intrinsic contact sensing principle formulated in (3).

There are some limitations to this study. First, the proposed method still requires fluctuations in the contact force at the beginning of estimation to estimate the tool shape accurately. As Figure 12 shows, less fluctuation before shape estimation converges results in worse contact-position estimation. This would be a theoretical limitation of methods using force signal-based inference. Second, the proposed

method must be extended to tools with more complex shapes. This requires a more efficient estimation and modified shape-estimation criteria. For instance, although the shape estimation criterion defined in (30) accelerates shape estimation, it assumes that there is only a single intersection point between the tool surface and the line of action defined in (3), making it inherently impossible to apply it to non-convex shapes. For practical applications, exception handling is also desired to reduce the impact of sudden changes in contact position or multiple points of contact on shape estimation, that affect adversely. Even with these weaknesses, however, this study demonstrated that the proposed method can estimate the tool shape with a large number of parameters only from force signals. We believe that this study has shown new development and challenges in force-signal processing.

We also have future works for a combination with robot controls. Improvement of accuracy would be needed for application to daily tasks, which sometimes require sub-centimeter accuracy. This could be achieved by a further research of the shape update rule. Force control to realize stable contact with the environment in the initial stages of estimation for estimation should be researched. Also, a control strategy that can reduce uncertain regions efficiently would make shape estimation faster than random contact as performed in this study. As the proposed method is based on probabilistic inference, it can be integrated with exploration strategies into a single probabilistic inference. This idea associates the proposed method with *control as inference* (Levine 2018) and *active inference* (Friston et al. 2016), which have garnered attention in the field of robotics. Besides, use of prior knowledge of other modalities, such as vision, would be desired to realize more rapid and stable estimation.

Conclusion

In this study, we propose a method for simultaneously estimating the contact position and tool shape using a grid representation. Using the proposed probabilistic model and shape parameter update method, the proposed method can estimate the shape representation with even more than 10^5 dimensions using only 300 particles. The proposed method was evaluated using simulations and experiments. Consequently, it can estimate the tool-shape geometry simultaneously with the contact positions. Moreover, owing to shape estimation, contact positions can be accurately estimated when the contact force does not fluctuate, which is impossible to achieve using the conventional methods without shape information or shape estimation.

Declaration of conflicting interests

The author(s) declared no potential conflicts of interest with respect to the research, authorship, and/or publication of this article.

Funding

This work was supported by JSPS KAKENHI Grant Number 22K14212.

Supplemental material

Supplemental material for this article is available online. The code is readily available at <https://doi.org/10.5281/zenodo.16949213>.

References

Akiba T, Sano S, Yanase T, Ohta T and Koyama M (2019) Optuna: A next-generation hyperparameter optimization framework.

Atkeson CG, An CH and Hollerbach JM (1986) Estimation of inertial parameters of manipulator loads and links. *The International Journal of Robotics Research* 5(3): 101–119. DOI:10.1177/027836498600500306.

Benallegue M, Gergondet P, Audrerr H, Mifsud A, Morisawa M, Lamiraux F, Kheddar A and Kanehiro F (2018) Model-based external force/moment estimation for humanoid robots with no torque measurement. In: *2018 IEEE International Conference on Robotics and Automation (ICRA)*. IEEE, pp. 3122–3129. DOI:10.1109/ICRA.2018.8460809.

Bicchi A (1990) Intrinsic contact sensing for soft fingers. In: *Proceedings., IEEE International Conference on Robotics and Automation*. IEEE Comput. Soc. Press, pp. 968–973. DOI:10.1109/ROBOT.1990.126117.

Bimbo J, Morgan AS and Dollar AM (2022) Force-based simultaneous mapping and object reconstruction for robotic manipulation. *IEEE Robotics and Automation Letters* 7(2): 4749–4756. DOI:10.1109/LRA.2022.3152244.

Chhatpar S and Branicky M (2005) Particle filtering for localization in robotic assemblies with position uncertainty. In: *2005 IEEE/RSJ International Conference on Intelligent Robots and Systems*. IEEE, pp. 3610–3617. DOI:10.1109/IROS.2005.1545286.

Featherstone R, Thiebaut S and Khatib O (1999) A general contact model for dynamically-decoupled force/motion control. In: *Proceedings 1999 IEEE International Conference on Robotics and Automation (Cat. No.99CH36288C)*. IEEE, pp. 3281–3286. DOI:10.1109/ROBOT.1999.774098.

Friston K, FitzGerald T, Rigoli F, Schwartenbeck P, O'Doherty J and Pezzulo G (2016) Active inference and learning. *Neuroscience & Biobehavioral Reviews* 68: 862–879. DOI:10.1016/j.neubiorev.2016.06.022.

Gadeyne K, Lefebvre T and Bruyninckx H (2005) Bayesian hybrid model-state estimation applied to simultaneous contact formation recognition and geometrical parameter estimation. *The International Journal of Robotics Research* 24(8): 615–630. DOI:10.1177/0278364905056196.

Galvez J, Gonzalez de Santos P and Pfeiffer F (2001) Intrinsic tactile sensing for the optimization of force distribution in a pipe crawling robot. *IEEE/ASME Transactions on Mechatronics* 6(1): 26–35. DOI:10.1109/3516.914388.

Grisetti G, Stachniss C and Burgard W (2005) Improving grid-based slam with rao-blackwellized particle filters by adaptive proposals and selective resampling. In: *Proceedings of the 2005 IEEE International Conference on Robotics and Automation*. IEEE, pp. 2432–2437. DOI:10.1109/ROBOT.2005.1570477.

Grisetti G, Stachniss C and Burgard W (2007) Improved techniques for grid mapping with rao-blackwellized particle filters. *IEEE Transactions on Robotics* 23(1): 34–46. DOI:10.1109/TRO.2006.889486.

Iwata H and Sugano S (2002) Whole-body covering tactile interface for human robot coordination. In: *Proceedings 2002 IEEE International Conference on Robotics and Automation (Cat. No.02CH37292)*. IEEE, pp. 3818–3824. DOI:10.1109/ROBOT.2002.1014315.

Julier SJ and Uhlmann JK (1997) New extension of the kalman filter to nonlinear systems. In: *SPIE Proceedings*. SPIE, pp. 182–194. DOI:10.1117/12.280797.

Karayiannidis Y, Smith C, Vina FE and Kragic D (2014) Online contact point estimation for uncalibrated tool use. In: *2014 IEEE International Conference on Robotics and Automation (ICRA)*. IEEE, pp. 2488–2494. DOI:10.1109/ICRA.2014.6907206.

Kim U, Jo G, Jeong H, Park CH, Koh JS, Park DI, Do H, Choi T, Kim HS and Park C (2021) A novel intrinsic force sensing method for robot manipulators during human–robot interaction. *IEEE Transactions on Robotics* 37(6): 2218–2225. DOI:10.1109/TRO.2021.3072736.

Kitamura H, Sakaino S and Tsuji T (2017) Contact point calculation on a haptic interface utilizing differentiated force. *IEEE Journal of Industry Applications* 6(2): 151–159. DOI:10.1541/ieejjia.6.151.

Koike R, Sakaino S and Tsuji T (2017) Contact point estimation in tactile interface using particle filter. In: *IECON 2017 - 43rd Annual Conference of the IEEE Industrial Electronics Society*. IEEE, pp. 8267–8272. DOI:10.1109/IECON.2017.8217451.

Kurita N, Sakaino S and Tsuji T (2012) Whole-body force sensation by force sensor with end-effector of arbitrary shape. In: *2012 IEEE/RSJ International Conference on Intelligent Robots and Systems*. IEEE, pp. 5428–5433. DOI:10.1109/IROS.2012.6386064.

Kutsuzawa K, Sakaino S and Tsuji T (2015) Estimation of individual contact force when two contact points exist during robotic tool use. In: *The Abstracts of the international conference on advanced mechatronics : toward evolutionary fusion of IT and mechatronics : ICAM*, volume 2015.6. Japan Society of Mechanical Engineers, pp. 46–47. DOI:10.1299/jsmeicam.2015.6.46.

Kutsuzawa K, Sakaino S and Tsuji T (2016) Estimation of individual force at three contact points on an end-effector by a six-axis force/torque sensor. In: *IECON 2016 - 42nd Annual Conference of the IEEE Industrial Electronics Society*. IEEE, pp. 6409–6414. DOI:10.1109/IECON.2016.7793932.

Kutsuzawa K, Sakaino S and Tsuji T (2017) A control system for a tool use robot: Drawing a circle by educing functions of a compass. *Journal of Robotics and Mechatronics* 29(2): 395–405. DOI:10.20965/jrm.2017.p0395.

Kutsuzawa K, Sakaino S and Tsuji T (2020) Simultaneous estimation of contact position and tool shape using an unscented particle filter. *IEEE Journal of Industry Applications* 9(5): 505–514. DOI:10.1541/ieejjia.9.505.

Levine S (2018) Reinforcement learning and control as probabilistic inference: Tutorial and review. *arXiv preprint* DOI:10.48550/arXiv.1805.00909.

Liang B, Liang W and Wu Y (2022) Parameterized particle filtering for tactile-based simultaneous pose and shape estimation. *IEEE Robotics and Automation Letters* 7(2): 1270–1277. DOI:10.1109/LRA.2021.3139381.

Manuelli L and Tedrake R (2016) Localizing external contact using proprioceptive sensors: The contact particle filter. In: *2016 IEEE/RSJ International Conference on Intelligent Robots and Systems (IROS)*. IEEE. DOI:10.1109/IROS.2016.7759743.

Mimura N and Funahashi Y (1994) Parameter identification of contact conditions by active force sensing. In: *Proceedings of the 1994 IEEE International Conference on Robotics and Automation*. IEEE Comput. Soc. Press, pp. 2645–2650. DOI:10.1109/ROBOT.1994.351115.

Murphy KP (1999) Bayesian map learning in dynamic environments. In: *Advances in Neural Information Processing Systems*. pp. 1015–1021.

Muto Sy and Shimokura Ki (1993) Accurate contact point detecting using force and velocity information complementarily. In: *[1993] Proceedings IEEE International Conference on Robotics and Automation*, volume 1. IEEE Comput. Soc. Press, pp. 738–744. DOI:10.1109/ROBOT.1993.292066.

Park J and Khatib O (2008) Robot multiple contact control. *Robotica* 26(5): 667–677. DOI:10.1017/S0263574708004281.

Petrovskaya A, Khatib O, Thrun S and Ng A (2006) Bayesian estimation for autonomous object manipulation based on tactile sensors. In: *Proceedings 2006 IEEE International Conference on Robotics and Automation, 2006. ICRA 2006*. IEEE, pp. 707–714. DOI:10.1109/ROBOT.2006.1641793.

Platt R, Permenter F and Pfeiffer J (2011) Using bayesian filtering to localize flexible materials during manipulation. *IEEE Transactions on Robotics* 27(3): 586–598. DOI:10.1109/TRO.2011.2139150.

Salisbury J (1984) Interpretation of contact geometries from force measurements. In: *Proceedings. 1984 IEEE International Conference on Robotics and Automation*, volume 1. Institute of Electrical and Electronics Engineers, pp. 240–247. DOI:10.1109/ROBOT.1984.1087180.

Thrun S, Burgard W and Fox D (1998) A probabilistic approach to concurrent mapping and localization for mobile robots. *Autonomous Robots* 5(3): 253–271. DOI:10.1023/A:1008806205438.

Tsuji T, Kaneko Y and Abe S (2009) Whole-body force sensation by force sensor with shell-shaped end-effector. *IEEE Transactions on Industrial Electronics* 56(5): 1375–1382. DOI:10.1109/TIE.2009.2014748.

Tsuji T, Seki T and Sakaino S (2017) Intrinsic contact sensing for touch interface with movable structure. *IEEE Transactions on Industrial Electronics* 64(9): 7342–7349. DOI:10.1109/TIE.2016.2633232.

Tsujimura T and Yabuta T (1989) Object detection by tactile sensing method employing force/torque information. *IEEE Transactions on Robotics and Automation* 5(4): 444–450. DOI:10.1109/70.88059.

van der Merwe R, Doucet A, de Freitas N and Wan E (2000a) The unscented particle filter. Technical report, Cambridge University Engineering Department.

van der Merwe R, Doucet A, de Freitas N and Wan E (2000b) The unscented particle filter. In: *Advances in Neural Information Processing Systems*, volume 13. MIT Press, pp. 584–590.

von Drigalski F, Taniguchi S, Lee R, Matsubara T, Hamaya M, Tanaka K and Ijiri Y (2020) Contact-based in-hand pose estimation using bayesian state estimation and particle filtering. In: *2020 IEEE International Conference on Robotics and Automation (ICRA)*. IEEE, pp. 7294–7299. DOI:10.1109/ICRA40945.2020.9196640.

Wan EA and van der Merwe R (2000) The unscented kalman filter for nonlinear estimation. In: *Proceedings of the IEEE 2000 Adaptive Systems for Signal Processing, Communications, and Control Symposium (Cat. No.00EX373)*. IEEE, pp. 153–158. DOI:10.1109/ASSPCC.2000.882463.